THE JOURNAL OF PHYSICAL CHEMISTRY B

Article

pubs.acs.org/JPCB

Mechanism of the Primary Charge Transfer Reaction in the Cytochrome bc_1 Complex

Angela M. Barragan,[†,‡] Klaus Schulten,[†,‡] and Ilia A. Solov'yov*[,§]

[†]Department of Physics, University of Illinois at Urbana−Champaign, 1110 West Green Street, Urbana, Illinois 61801, United States

[‡]Beckman Institute for Advanced Science and Technology, University of Illinois at Urbana−Champaign, 405 North Mathews Avenue, Urbana, Illinois 61801, United States

[§]Department of Physics, Chemistry and Pharmacy, University of Southern Denmark, Campusvej 55, DK-5230 Odense M, Denmark

Supporting Information

ABSTRACT: The bc_1 complex is a critical enzyme for the ATP production in photosynthesis and cellular respiration. Its biochemical function relies on the so-called Q-cycle, which is well established and operates via quinol substrates that bind inside the protein complex. Despite decades of research, the quinol−protein interaction, which initiates the Q-cycle, has not yet been completely described. Furthermore, the initial charge transfer reactions of the Q-cycle lack a physical description. The present investigation utilizes classical molecular dynamics simulations in tandem with quantum density functional theory calculations, to provide a complete and consistent quantitative description of the primary events that occur within the bc_1 complex upon quinol binding. In particular, the electron and proton transfer reactions that trigger the Q-cycle in the bc_1 complex from *Rhodobacter capsulatus* are studied. The coupled nature of these charge transfer reactions was revealed by obtaining the transition energy path connecting configurations of the Q_o-site prior and after the transfers. The analysis of orbitals and partial charge distribution of the different states of the Q_o-site has further supported the conclusion. Finally, key structural elements of the bc_1 complex that trigger the charge transfer reactions were established, manifesting the importance of the environment in the process, which is furthermore evidenced by free energy calculations.

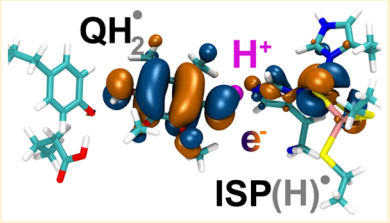

INTRODUCTION

Cellular respiration and photosynthesis constitute the most fundamental energy conversion processes for sustaining living cells. These two processes rely on a series of energy transport events, where the electron and proton transfer reactions are the primary tools for energy transfer across the cellular energetic apparatus. One of the key elements involved in bacterial photosynthesis and mitochondrial respiration, which utilizes such electron and proton transfer reactions to effectively create a transmembrane proton gradient, is the bc_1 complex.[1−3]

The bc_1 complex is a catalytic transmembrane protein that, by a series of proton and electron transfer reactions, oxidizes quinol (QH_2) cofactors at the so-called Q_o active site and reduces quinone (Q) cofactors at the Q_i active site, in an overall process referred to as the Q-cycle.[4] The initial step of the Q-cycle corresponds to the binding of a QH_2 molecule to the Q_o-site followed by two electron transfer reactions, taking place in a bifurcated manner, toward different prosthetic groups of the bc_1 complex subunits. As depicted in Figure 1, one electron is transferred to the heme c_1 of the cytochrome (cyt.) c_1 subunit via the Fe_2S_2 cluster of the iron−sulfur protein (ISP) subunit, while a second electron is transferred to heme b_H via heme b_L of the cyt. b subunit.[3] During each QH_2 oxidation, the bifurcated electron transfer occurs alongside two proton transfers from the QH_2 to the positive side of the membrane, in order to create a transmembrane potential that is necessary for ATP synthesis.[4]

The mechanism of the proton and electron transfers at the Q_o-site of the bc_1 complex still remains elusive. However, it is believed that the bifurcation of the electrons is accompanied by the proton transfers, i.e., that electrons and protons are transferred simultaneously from QH_2 to the bc_1 complex in a coupled fashion.[5,6] In fact, such proton-coupled electron transfer (PCET) reactions are common in various biological systems,[7,8] but it has not been proven for the bc_1 complex yet. In this study, we investigate the possibility of coupled charge transfer reactions at the Q_o-site of the bc_1 complex from *Rhodobacter capsulatus*,[9] and demonstrate the feasibility of the PCET process.

Previous investigations of the bc_1 complex based on molecular dynamics (MD) simulations and quantum chemistry (QC) calculations have revealed two feasible QH_2 binding motifs at the Q_o-site,[10] giving rise to the possibility of two different charge transfer models. The two models, models I and II, differ in the protonation state of the Fe_2S_2-bound residue H156 (numbering is consistent with the crystal structure of the ISP subunit of the *Rhodobacter capsulatus* bc_1 complex[9]), which is one of the key elements involved in the QH_2 binding and, as it will be evidenced in this study, in the subsequent charge transfer reactions at the Q_o-site. The Q_o-site for both models is

Received: July 23, 2016
Revised: September 11, 2016
Published: September 23, 2016

DOI: 10.1021/acs.jpcb.6b07394
J. Phys. Chem. B 2016, 120, 11369−11380

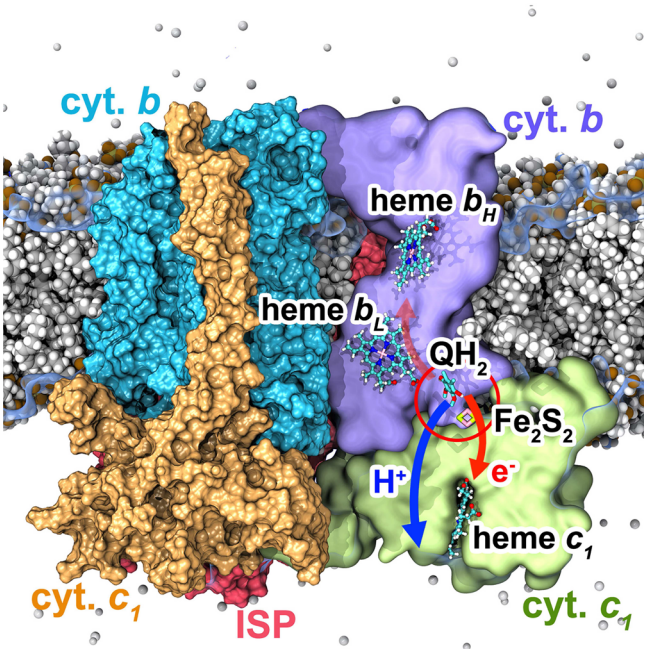

Figure 1. *Rhodobacter capsulatus* bc_1 complex. The interior of the cytochrome bc_1 complex, shown here as embedded in a bilayer lipid membrane, consists of hemes and iron−sulfur (Fe_2S_2) clusters that participate in the charge transfer reactions of the Q-cycle. The left monomer of the bc_1 complex shows the exterior surface of the protein subunits, while the right monomer, transversally cut, shows the internal cofactors heme b_H, heme b_L, Fe_2S_2, heme c_1, and a bound quinol (QH_2) substrate at the Q_o-site (red circle). The bound substrate initiates the Q-cycle through primary proton and electron transfer reactions, schematically shown by blue and red arrows, respectively.

featured in Figure 2. This figure depicts the differences between the two models, in particular, the varied protonation state of the H156 residue and the impact it has on the charge transfer pathways.[11]

The primary charge transfer reactions at the Q_o-site involve one electron and one proton transfer from QH_2 to their bc_1 complex acceptor sites,[12,13] and in general, these two processes can occur either sequentially or simultaneously. The possible scenarios in the deprotonated-H156 model I and protonated-H156 model II are schematically illustrated below.

Model I:

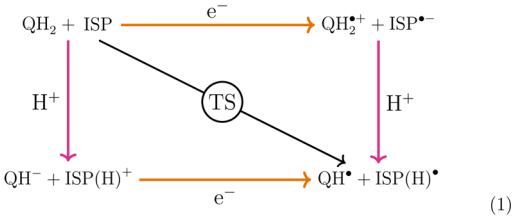

(1)

Model II:

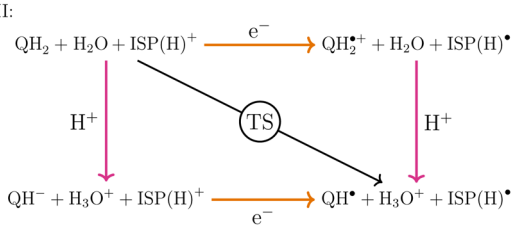

(2)

Since the residue H156 is considered deprotonated in model I, the proton from QH_2 can be transferred directly to H156;

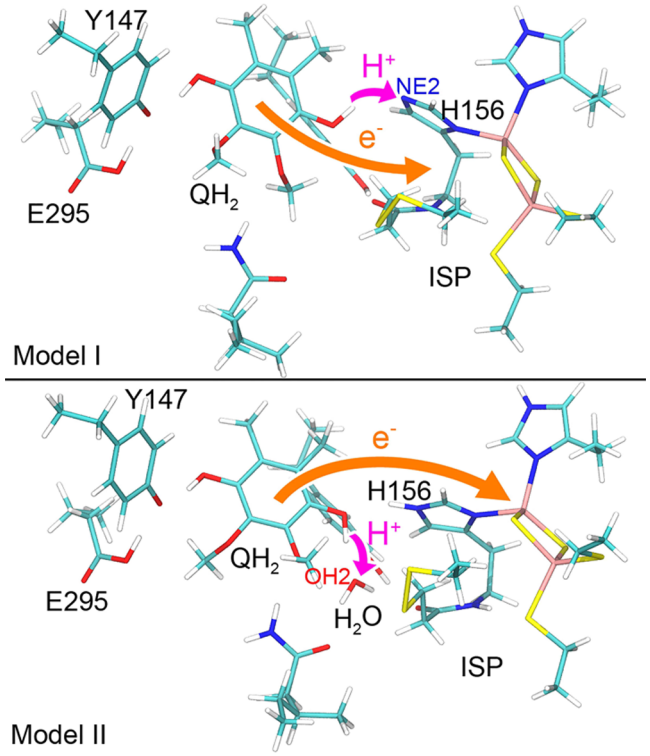

Figure 2. Primary charge transfer reactions at the Q_o-site of the bc_1 complex. Initial configuration of the Q_o-site of the bc_1 complex, showing residues and the QH_2 substrate, prior to the charge transfer reactions. The upper panel (model I) shows the quantum mechanically optimized structure of the Q_o-site in the case of a deprotonated H156 residue. The lower panel (model II) shows the Q_o-site in an optimized state where H156 is protonated and a water molecule coordinates the QH_2 binding. The orange and magenta arrows illustrate schematically the paths for the primary electron and proton transfers of the Q-cycle. Orange arrows point toward the Fe_2S_2 cluster, while magenta arrows point toward the proton acceptor atoms NE2 and OH2 in model I and model II, respectively.

however, in model II, the protonated H156 suggests a proton transfer to a different residue, which in previous investigations[11,14] was thought to be a H_2O molecule. The redox changes of the QH_2 and ISP fragments are depicted in models I and II as orange and magenta arrows, corresponding to electron and proton transfers, respectively. The models illustrate sequential charge transfer reactions, leading to intermediate states with a charged semiquinone and ISP. In the case of model I, only QH_2 and ISP change their redox states during the transfers, while in model II an additional water molecule, which acts as an intermediate proton acceptor, is involved. This water molecule is, therefore, included in the reaction scheme of model II. The diagonal arrows in models I and II illustrate the possibility of simultaneous electron and proton transfers, corresponding to the PCET regime, that undergoes a transition state (TS). Such a TS corresponds to a state in which both charges have started to be transferred from QH_2 to their corresponding acceptors, but these are not yet considered in a final state.

The present investigation supports the hypothesis of a possible PCET reaction as the primary reaction occurring upon quinol binding at the Q_o-site of the bc_1 complex: exploration of all possible states portrayed in models I and II allowed the coupled character of the charge transfer processes to be

DOI: 10.1021/acs.jpcb.6b07394
J. Phys. Chem. B 2016, 120, 11369−11380

Table 1. Summary of Performed MD Simulations and QC Calculations[a]

type	Q_o-site redox state	Q_o-site charges	simulation time (ns)
1. MD	reactant	CHARMM36 FF	360
2. QC	reactant	e^- at donor, H^+ at donor	
	TS	e^-, H^+ delocalized	
	e^- transfer only	e^- at acceptor, H^+ at donor	
	H^+ transfer only	e^- at donor, H^+ at acceptor	
	product	e^- at acceptor, H^+ at acceptor	
3. MD	reactant	CHARMM36 refined FF	80
	product	CHARMM36 refined FF	80

[a]Calculations are listed according to the redox state of the system. MD simulations were performed for all atoms (including protein, cofactors, water, lipids, and ions), while QC calculations were performed for a selection of atoms in the Q_o-site, as shown in Figure 2 and described in the text. Initial MD simulations were performed for the bc_1 complex in its reactant state in order to obtain an equilibrated configuration of the system.[10] The QC calculations are classified according to the localization of the electron (e^-) and proton (H^+) at either the QH_2 (donor) or H156/H_2O (acceptor), reproducing all possible states in models I and II. Concluding 80 ns long MD simulations were performed using the refined force fields (FF), obtained from the QC calculations of the Q_o-site residues in the reactant and product states.

revealed. Through an accurate calculation of the reaction energy profiles, the initial state (reactant), TS, and final state (product) of the bc_1 complex Q_o-site were established. The analysis of molecular orbitals, charge delocalization, and electrostatic properties for the reactant and product states evidenced furthermore the coupled nature of the proton and electron transfers and allowed the driving force that stimulates the charge transfer reactions at the Q_o-site in the two different binding scenarios of the quinol substrate to be determined.

METHODS

The primary charge transfer reactions occurring at the Q_o-site of the bc_1 complex were characterized through an in-depth analysis of MD simulations combined with QC calculations of the two different configurations of the complex, corresponding to models I and II introduced in Figure 2. The calculations, performed for models I and II, were divided into three main stages, summarized in Table 1. First, MD simulations of the entire system in the reactant state[10] allowed an equilibrated configuration of the bc_1 complex to be obtained that describes its initial state prior to charge transfer reactions and, therefore, is considered optimal for QC analysis. Second, QC calculations were performed for a selected fragment of the bc_1 complex, composed of the residues largely involved in the charge transfer reactions and the QH_2 headgroup, as shown in Figure 2. Finally, by using the atomic charges obtained from the QC calculations, a refined reactant as well as a product state of the entire system were simulated dynamically to acquire sufficient conformational statistics for describing the PCET free energy calculations.

All of the MD simulations were performed employing NAMD 2.11[15] utilizing the CHARMM36 force field with CMAP corrections[16] for the proteins. The QC calculations were carried out with the Gaussian 09 package,[17] employing the UB3LYP DFT method,[18] widely used previously in iron−sulfur containing system optimizations.[19−25] All images of the bc_1 complex, including molecular orbitals and electrostatic potentials, were obtained with VMD 1.9.2.[26] Technical details of the methods employed in the calculations are described below.

MD Simulations prior to Charge Transfer Reactions. In an earlier study,[10] 360 ns long MD simulations were performed for the bc_1 complex represented through models I and II, allowing the bc_1 complex, with a bound QH_2 at the Q_o-site, to equilibrate first and then reach a stable conformation prior to the PCET reaction.

For modeling of the system in VMD 1.9.2,[26] the X-ray crystal structure of the bc_1 complex of *Rhodobacter capsulatus* (PDB ID: 1ZRT)[9] was embedded in a bilayer membrane, composed of 102 cardiolipin (CL 18:2/18:2/18:2/18:2), 406 phosphatidylcholine (PC 18:2/18:2), and 342 phosphatidylethanolamine (PE 18:2/18:2) lipids to represent a mitochondrial membrane.[14] The lipid membrane with the embedded protein was solvated within a TIP3P water box at a salt (NaCl) concentration of 0.05 mol/L, and neutralized with salt ions. The *Rhodobacter capsulatus* crystal structure originally contained stigmatellin and antimycin molecules bound at the Q_o- and Q_i-sites, respectively, while the substrate molecules for the Q-cycle are QH_2 and Q. The Q and QH_2 molecules were thus aligned to the original antimycin and stigmatellin positions. The total simulation system consisted of 500,791 atoms in model I and 502,165 atoms in model II, including proteins with cofactors, substrate molecules, lipids, water molecules, and ions.

Addition of the hydrogen atoms that are missing in the crystal structure of the bc_1 complex was performed with the VMD plugin psfgen.[26] Standard charges and topologies of the bc_1 complex proteins were assumed, in accordance with the CHARMM36 force field. However, parameters for the prosthetic groups, hemes, and Fe_2S_2 cluster were adopted to be consistent with earlier investigations,[14,27] in which the groups are considered prior to PCET, i.e., in the oxidized form. Charges and topology of the QH_2 and Q cofactors were taken from an earlier study.[27] The standard CHARMM36 force field was employed[28] for the PE and PC lipids, as well as for lipid tails of CL. The CL headgroup charges and parameters were adopted from an earlier investigation.[29]

All histidine residues of the bc_1 complex were considered as δ-protonated except for H156, which has been assumed deprotonated in model I and ϵ-protonated in model II. Inspection of the bc_1 complex crystal structure suggested disulfide bonds between the C144 and C167 residues from cyt. c_1 and between C138 and C155 residues from ISP. Both disulfide bonds were included in both computational models.

The simulations were performed in the NVT ensemble, where the temperature was kept at 310 K. The long-range electrostatic interactions were calculated, by employing periodic boundary conditions using the PME method,[28] with a smooth cutoff of 12 Å; the same cutoff was used for van der Waals interactions. All MD simulations were performed with a time

DOI: 10.1021/acs.jpcb.6b07394
J. Phys. Chem. B 2016, 120, 11369−11380

step of 2 fs, and following a simulation protocol in which the system was equilibrated while keeping constraints on selected atoms: (i) first all protein backbone, (ii) then highly movable non-transmembrane segments of the ISP and cyt. c_2 subunits, and (iii) finally releasing all the atoms.

The trajectories obtained in an earlier investigation[10] were utilized to analyze the reactant state of the bc_1 complex and determine the driving force that the environment exerts on the transferring charges at the Q_o-site. For this purpose, the analysis of the electrostatic potential was performed on a smoothed electrostatic potential grid, calculated by using the PMEPOT plugin[30] in VMD, using the entire 360 ns long MD trajectories for model I and model II.

QC Calculations. The QC calculations included the residues and cofactors involved in the charge transfer reactions, selected from the model systems previously equilibrated during the 360 ns MD simulations. The set of residues, shown in Figure 2, constitutes the computational models of the Q_o-site and was selected on the basis of criteria such as proximity to the quinol headgroup, proximity to the Fe_2S_2 cluster, and the residue charge. These selection criteria guaranteed the inclusion of the charge donor and charge acceptor residues, as well as all charged or polar residues that would largely contribute to the driving forces during the charge transfer process.

The computational model of the Q_o-site consisted of 168 atoms for model I and 172 atoms for model II, including the QH_2 headgroup, Fe_2S_2 cluster, and pre-equilibrated side chains of cyt. *b* residues Y147, I292, E295, and Y302 and of ISP residues C133, H135, C138, C153, C155, and H156. In model II, a H_2O molecule was additionally included in the QC calculations, as it corresponded to the most probable intermediate proton acceptor[10] in this particular case. The C_α atoms of the side chain residues were replaced by CH_3 groups, employing for this purpose the MOLEFACTURE plugin of VMD.[26]

All of the QC calculations employed two standard 6-31G(d) and 6-311G(d) basis sets to expand the electronic wave functions. The simpler 6-31G(d) basis set was used to efficiently find optimized reactant and product states of the Q_o-site, and then, more refined calculations were performed with the 6-311G(d) basis set, as it describes more accurately systems with heavy atoms, such as Fe and S, due to its triple-ζ accuracy and additional diffuse functions.[31] The comparison of results obtained with the two basis sets is provided in the Supporting Information. Initial QC geometry optimizations of the Q_o-site model in the reactant state were performed, and in order to avoid an unphysical collapse of the atoms, the C_α atom positions, taken from the pre-equilibrated structure, were kept fixed during the optimization calculations.

In order to consider the possible sequential and concerted pathways of the electron and proton transfers during the primary charge transfer reactions at the Q_o-site, see models I and II, the system was set up in all possible redox states that it could populate during single or coupled charge transfers from QH_2 to their respective acceptors (see Table 1). QC geometry optimizations were performed for all the single-transfer states. The transition states (TSs) were obtained through the synchronous transit-guided quasi-Newton (STQN) method[32,33] in Gaussian 09.[17] Additional confirmation of the TS for the PCET was made throughout vibrational frequency calculations followed by intrinsic reaction coordinate (IRC) integration,[34,35] also performed in Gaussian 09.

Once the TSs for the two models were established, QC geometry optimizations were carried out from these states toward the reactant and product configurations of the Q_o-site, generating a reaction path (energy profile) for the PCET reactions. A total of 31 configurations of the Q_o-site were selected from these paths for each model, including the TS, product, and reactant states for further analysis, such as the calculations of molecular orbitals and atomic charges, derived following the ESP Merz−Singh−Kollman scheme.[36,37]

The ESP fitted charges were used for redefining the atomic charges of Q_o-site residues, allowing consequent MD simulations to be performed for the bc_1 complex in the reactant and product states. For this purpose, Q_o-site residues were redefined, allowing the topology files needed for MD simulations with refined charges to be updated, corresponding to the Q_o-site in the reactant and product states. During the charge fitting process, charge symmetries were taken into account and only the atomic charges of the residue side chains were reassigned, while the charges of polypeptide backbone atoms were kept at the standard CHARMM36 force field values.[38] The modified atomic charges, used in the MD simulations, are provided in the Supporting Information.

To stress the influence of Y147 and E295 on the PCET reaction, additional QC calculations of the system were performed for two alternate configurations where (i) Y147 was replaced by a H_2O molecule and (ii) where both residues Y147 and E295 were removed.

MD Simulations after PCET. MD simulations were performed for the bc_1 complex in the reactant and product states, utilizing the refined topology files obtained by reassigning the atomic charges of the Q_o-site residues with the ESP charges taken from the QC calculations (see Table 1). By employing the modified charges, 80 ns long MD simulations, in the NVT ensemble, were performed using NAMD 2.11, for the bc_1 complex model I. All of the simulation parameters, such as temperature, interaction cutoff distances, ion concentration, and others, were the same as in the initial 360 ns long MD simulations. The 80 ns long MD trajectories were used to sample the total energy of the system in the different redox states and to carry out a statistical analysis of energy differences of the system in the reactant and product states. The energy differences were evaluated using Mathematica 10.3[39] and allowed to establish the free energy profile for the charge transfer reactions in model I.

RESULTS AND DISCUSSION

Earlier studies[10,11,14] suggest that two QH_2 binding motifs at the Q_o-site of the bc_1 complex from *Rhodobacter capsulatus* are plausible, differing in the protonation state of the residue H156 of the ISP, as shown in Figure 2. For both binding motifs, referred to as model I for H156 deprotonated and model II for H156 protonated, the primary electron and proton transfer reactions at the Q_o-site were studied through an in-depth MD and QC analysis, allowing the energetics of the reactions and the nature of the proton and electron transfers to be established. For this purpose, TSs, corresponding to different charge transfer pathways, were obtained for model I and model II. From the calculated TSs, the charge transfer reaction pathways were revealed by scanning the potential energy surfaces along the charge transfer reaction coordinate. For a particular case of PCET reaction, analysis of the charge delocalization, electrostatic potential at the Q_o-site, and free energy calculations allowed one to identify the key residues

DOI: 10.1021/acs.jpcb.6b07394
J. Phys. Chem. B 2016, 120, 11369−11380

involved in the charge transfer reaction and to establish the corresponding driving forces.

TS of the Charge Transfer Reaction. The TS for a molecular system separates the final state (product) from the initial state (reactant) on the potential energy landscape of a chemical reaction. Thus, once the TS of a reaction is identified, it is possible to follow a reaction coordinate in two opposite directions, starting from the TS and, thereby, to reconstruct the energy profile of the reaction. Finding the reactant, transition, and product states is key in the description of the reaction mechanism, as it allows one to establish the activation energy E_A and the reaction energy ΔE, and hence to characterize the reaction itself.

By performing QC geometry optimizations over all the states depicted in models I and II, investigations of possible sequential and simultaneous electron and proton transfers at the Q_o-site of the bc_1 complex were carried out. Despite all of the efforts, intermediate states, in which either the electron or the proton had been transferred, could not be established, since the system always relaxed to either the initial state, in which neither charge has been transferred, or the final state, in which both charges have been transferred simultaneously; i.e., only reactant and product states could be established. These results hint strongly that only a simultaneous reaction, in which the electron and the proton are transferred in a concerted manner, is feasible at the Q_o-site, as indicated by diagonal arrows in models I and II, and that the reaction coordinate corresponds to the diagonal route in the models.

In contrast, the TSs for the concerted reactions were established for model I and model II, thus allowing the reactant and product states to be reconstructed and revealing the energy landscapes of PCET reactions. Figure 3 shows the energy profiles calculated for the two models of the Q_o-site and indicates the TSs, which corresponds to the highest energy values of the profile in each model, as well as the initial and final electronic configuration of the Q_o-site.

As indicated in Figure 3, model I reactants correspond to a bound QH_2 and ISP residues and cofactors (labeled as ISP···QH_2), while model II reactants correspond to a bound QH_2 to ISP(H^+), representing the ISP subunit with a protonated H156 residue and, additionally, a quinol-binding H_2O molecule (labeled as ISP(H^+)···QH_2+H_2O). Products in both models correspond to a radical semiquinone $QH^\bullet$, an ISP(H)$^\bullet$, and, only in the case of model II, an additional hydronium ion H_3O^+ is present.

Energetics of the Charge Transfer Reactions. The intrinsic differences in the molecular structure of the charge acceptors between the two studied computational models determine the pathway of the proton transfer from QH_2 to the bc_1 complex. In model I, the proton is transferred to H156 of the ISP, leading to the formation of a radical ISP(H)$^\bullet$; however, as per a protonated H156 in model II, the proton is transferred to an acceptor H_2O molecule, leading to the creation of a hydronium ion H_3O^+, in addition to the ISP(H)$^\bullet$ radical that is being formed by the electron transfer to the initial ISP(H)$^+$. Such differences in the reaction mechanism manifest as differences in the reaction energy profiles, demonstrated by the activation energy, E_A, and reaction energy, ΔE, in Figure 3.

In both considered models, the energy of the reactant state is lower than the energy of the product state, indicating that the associated charge transfer reactions are uphill processes. This means that the reactions can occur backward, bringing the charges back to the initial QH_2 donor, even after the initial transfers have occurred. The probability of this back transfer to happen is, however, higher in the case of model II than in the case of model I, where the difference $E_A - \Delta E$ is considerably higher (see Table 2).

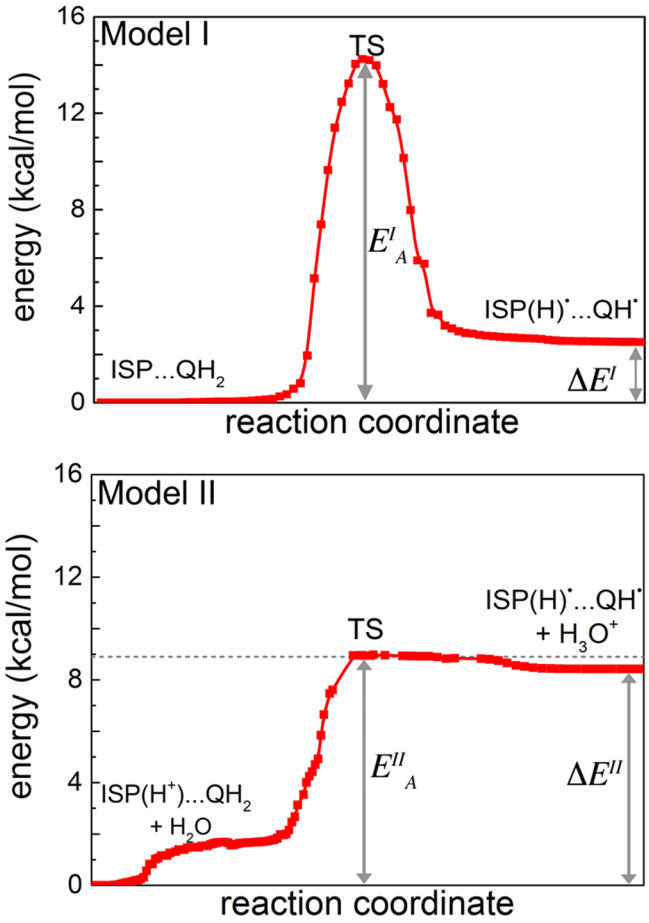

Figure 3. Energetics of the primary charge transfer reactions at the Q_o-site of the bc_1 complex. The energy profiles of the PCET reactions are obtained through QC optimizations of the two studied Q_o-site models (see Figure 2), starting from the TS by using the B3LYP/6-311G(d) method. The upper panel (model I) describes the PCET between the QH_2 substrate and the ISP with initially deprotonated H156 residue. The lower panel (model II) shows the energy of a PCET where the H156 residue of the ISP is initially protonated. E^I_A and E^{II}_A correspond to the activation energies of the reactions in the case of models I and model II, respectively, while ΔE^I and ΔE^{II} indicate the reaction energies. Labels indicate the redox states of the initial reactants and reaction products in each model.

Table 2. Activation Energy and Reaction Energies[a]

energy (kcal/mol)	model I	model II
E_A	14.20	8.94
	(14.93)	(12.79)
ΔE	2.51	8.42
	(4.17)	(12.73)
$E_A - \Delta E$	11.69	0.52
	(10.76)	(0.06)

[a]Energies, indicated in Figure 3, were computed for models I and II through QC calculations carried out with the B3LYP/6-311G(d) and B3LYP/6-31G(d) methods. The B3LYP/6-31G(d) values are shown in parentheses.

DOI: 10.1021/acs.jpcb.6b07394
J. Phys. Chem. B 2016, 120, 11369−11380

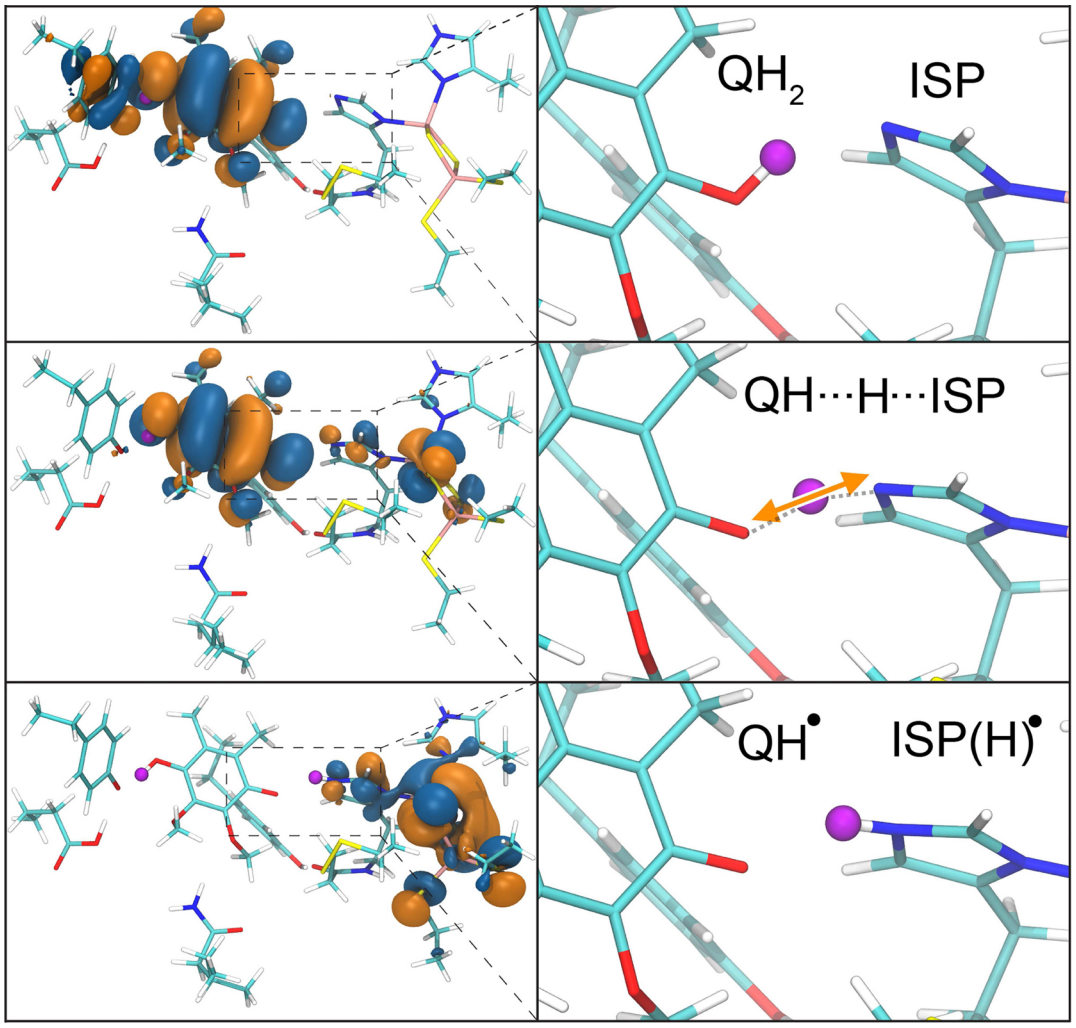

Figure 4. Electron and proton transfers at the Q_o-site of the bc_1 complex. Optimized configurations of the bc_1 complex Q_o-site during the PCET in model I: reactant state (upper panels), TS (middle panels), and product state (lower panels). Left panels show the molecular orbital undergoing a significant change upon the charge transfer reaction. Right panels show a zoom into the Q_o-site with QH_2 and ISP highlighted; the magenta sphere represents a proton that undergoes a transfer from QH_2 to the ISP, and is shared by both reaction partners in the TS (middle panel). The reaction coordinate of the charge transfer reaction (see Figure 3) corresponds to the displacement path of this proton, and is confirmed by an imaginary oscillation mode in the TS (orange arrow).

Table 2 summarizes the activation and reaction energies obtained from the QC calculations, as well as the difference $E_A - \Delta E$ for both studied models of the Q_o-site. The activation energies are 14.20 and 8.94 kcal/mol for model I and model II, respectively. This comparison suggests that the PCET is more likely to occur in a configuration of the system described by model II, with a protonated H156 residue. Such a difference has a direct impact on the kinetics of the charge transfer reactions,[40] leading to a higher PCET rate constant in the case of model II than in the case of model I. However, the rate constants of the reverse charge transfer reaction have to be taken into account in order to establish the stability of the PCET process. The rate constant for the reverse reaction in the case of model II also depends on the diffusivity of H_3O^+, which is the proton carrier in this case. The diffusion of the hydronium ion away from the Q_o-site could assist the prevention of the proton transfer in the reverse reaction, even though the low energy barrier of the reverse reaction in the case of model II makes it favorable to occur.

As listed in Table 2, the barriers for the back reactions, $E_A - \Delta E$, differ for both models, being equal to 11.69 kcal/mol for model I and 0.52 kcal/mol for model II, respectively, strongly affecting the reaction kinetics, namely, the stability of the product state after the PCET. In model I, $E_A - \Delta E$ is considerably larger than this in the case of model II: a small energy barrier in the case of model II reveals that the system is equally likely to populate the TS and the product state, making the latter a rather unstable state of the system, and allowing a proton transfer back toward its initial donor QH_2.

The observed difference between the two models is primarily attributed to the fact that the proton acceptor in the case of model II is a solvent H_2O molecule, as opposed to model I where the acceptor is the H156 residue. Even though model I seems to represent a more stable product state, it is possible that the hydronium is necessarily formed as an initial proton transporter to be translocated across the membrane. Previous studies[10,14] suggest this possibility, and here it is evidenced to still be a plausible scenario.

Table 2 summarizes the energies calculated by using the B3LYP/6-31G(d) method with a double-ζ precision basis set. All calculations were carried out using the triple-ζ B3LYP/6-311G(d) and double-ζ B3LYP/6-31G(d) basis sets for the

DOI: 10.1021/acs.jpcb.6b07394
J. Phys. Chem. B 2016, 120, 11369−11380

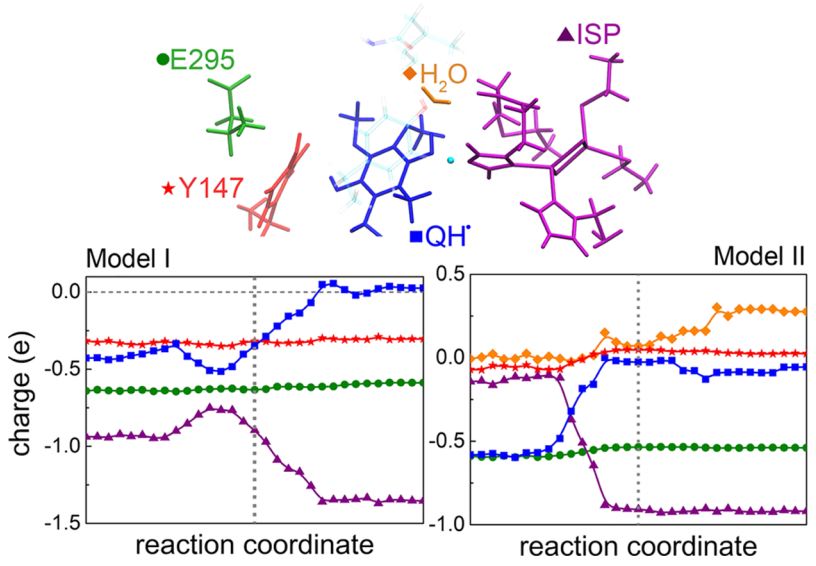

Figure 5. Charge delocalization at the Q_o-site of the bc_1 complex. ESP charges calculated as a function of the reaction coordinate for Q_o-site fragments, for model I (left panel) and model II (right panel). The upper panel defines colors used to distinguish between individual fragments at the Q_o-site. Due to the difference in the two models, the ISP fragment (magenta) has an additional proton in the case of model II; thus, the initial charge of this fragment is ∼ −1.0 e and ∼0 e for model I and model II, respectively. The coordinating water molecule (orange) is present only in model II. The partial charge of the H^+ proton (light blue sphere), which is seen detached from QH_2, is not included in the calculation. The vertical dotted gray line indicates the reaction coordinate at the TS.

purpose of testing the accuracy of different methods. A comparison of the calculations for the two basis sets is given in the Supporting Information. A relatively small difference in energies, shown in Table 2, computed with different methods, suggests that both methods could actually be used to describe the studied PCET reactions.

Reactant and Product States of the PCET. Structurally, the TS of the PCET occurring at the Q_o-site corresponds to a quinol-donor hydrogen H2 shift toward its acceptor atom, NE2 of H156 in the case of model I or OH2 of the H_2O molecule in the case of model II (see Figure 2), accompanied by a redistribution of the transferring electron between the donor, QH_2, and acceptor, Fe_2S_2. However, in the reactant and product states, the transferring charges are well localized in their specific donor and acceptor residues. In the reactant state, the electron is localized at the donor, QH_2 site, and the proton (H2 atom) is bonded to it, while in the product state, the proton is bonded to the acceptor, H156 or H_2O (in model I and model II, respectively), and the electron is localized at the Fe_2S_2 cluster site. Snapshots of the product, transition, and reactant states in model I are depicted in Figure 4, where the hydrogen atom, highlighted as a magenta sphere, depicts the transferring proton, and the calculated highest occupied molecular orbital (HOMO), in orange and blue, illustrates the transferring electron.

The hydrogen atom is localized equidistant from its donor, QH_2, and acceptor, H156, in the TS (middle panel), and appears bonded to the donor (upper panel) and the acceptor (lower panel) in the reactant and product states, respectively. The orange arrow shown atop the hydrogen atom corresponds to the imaginary normal vibration mode, obtained through QC calculations for the TS. A single imaginary frequency in the normal vibration spectrum was revealed by the B3LYP/6-311G(d) calculation, indicating a first order TS which hints on the proper reaction coordinate, and indicates a bond breakage of the donor−proton bond, as expected in a TS.[41] The vibration mode involves the motion of the H atom along the line connecting the donor and acceptor sites. The delocalization of the HOMO evidences a partially transferred electron in the TS, while a well localized HOMO at the donor and acceptor sites can be seen for the reactant and product states, respectively.

Molecular Orbitals Redistribution upon Charge Transfer. The coupled nature of the primary charge transfer reaction at the Q_o-site of the bc_1 complex can be described through a quantum mechanical analysis of the electronic structure and atomic spatial distribution studied along the reaction path.

For this purpose, the electronic distribution at the Q_o-site was calculated for the 31 selected configurations, following the reaction profile in Figure 3. The HOMO, computed for each configuration, allowed the distribution of the valence electrons at the donor and acceptor sites during the charge transfer reaction to be visualized. Most of the remaining occupied molecular orbitals exhibit minor perturbations. The HOMO calculated for the 31 configurations, is displayed in a movie (see the Supporting Information), which features the reaction pathway dynamically. Figure 4 shows the HOMO, calculated for the initial, transition, and final states of the Q_o-site in model I. Initially, the HOMO is localized around the QH_2 substrate headgroup, while it shifts toward the ISP upon the charge transfer reaction; the TS features electron delocalization between QH_2 and ISP, as it is expected during an electron transfer.[42]

HOMO delocalization in the TS of the two computational models, suggests that in the course of the charge transfer reaction the system features charge delocalization throughout the different residues of the Q_o-site. An analysis of the atomic charge assignments provides a more quantitative description of such delocalization and hence a more accurate characterization of the reaction mechanism.

Charge Distribution at the Q_o-Site. Through QC calculations, the atomic charges were obtained for each of the 31 selected configurations. Figure 5 shows the total ESP-fitted charges computed for the residues of the Q_o-site in the case of

DOI: 10.1021/acs.jpcb.6b07394
J. Phys. Chem. B 2016, 120, 11369−11380

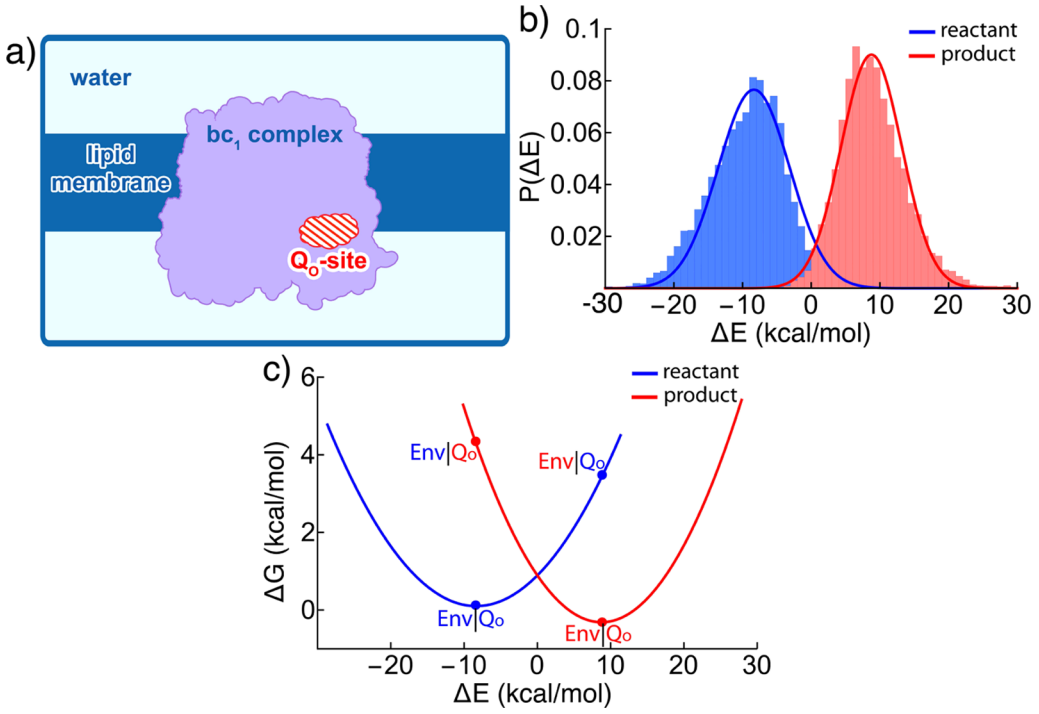

Figure 6. Free energy differences of the PCET. (a) The Q_o-site of one of the bc_1 complex monomers is indicated schematically by a red striped area in order to differentiate it from its molecular environment, which is composed of water, the lipid membrane and the remaining bc_1 complex. The PCET process is described through four different configurations of the system, where the Q_o-site and its molecular environment were individually assumed to resemble the reactant and the product states of the bc_1 complex. (b) The distributions $P(\Delta E)$ of the energy differences ΔE between the two configurations of the bc_1 complex, before and after the PCET reaction, assuming that the molecular environment of the Q_o-site resembles the reactant (blue) and product states (red). The energy differences are calculated using eqs 5 and 6. (c) The free energy differences of the PCET process in the bc_1 complex were calculated, for the reactant (blue) and the product (red) states of the Q_o-site, from the probability distributions shown in part b according to eq 7. Colored labels on the plot identify the four configurations of the Q_o-site (Q_o) and its molecular environment (Env) for which the total energy of the system was sampled; blue color indicates that Q_o or Env are in the reactant state of the bc_1 complex, while red color indicates these parts of the system are in the product state.

model I and model II. With exception of the transferring proton charge, the atomic charges are summed into fragments to illustrate the effect of charge exchange at the Q_o-site during the charge transfer reactions. The residues at the Q_o-site are colored by fragments (upper panel), for which the total charge is calculated as a function of the reaction coordinate (lower panels). In both models, charge delocalization is evidenced given a specific molecular structure: in model I, a negative charge is transferred from the QH_2 substrate (blue) to the ISP (magenta), while keeping a nearly constant charge distribution in the Y147 (red) and E295 (green) residues. The transference of charges during the reaction is described through stepwise changes in the total charge of the donor and acceptor molecules upon the change of the reaction coordinate.

In model I, one notes a symmetrical change of charge of the total charge of the $QH^{\bullet}$ and ISP fragments, see blue and magenta and lines in Figure 5, which provides the evidence of the electron transfer reaction between the QH_2 and ISP fragments. In model II, however, the existence of a coordinating H_2O molecule in the Q_o-site affects the charge transfer between QH_2 and ISP, showing a slight asymmetry in the total charge of these fragments. Furthermore, a slight increase of the orange line indicates that the total charge of the H_2O fragment (proton acceptor) increases simultaneously as the charge of the ISP fragment (electron acceptor) decreases.

The difference in the initial total charge of the ISP fragment for both computational models is due to the difference in the protonation state of the residue H156, which makes the initial total charge of the ISP in model I ~ -1.0 e and that in model II $\sim$0 e. In both models, the Y147 and E295 residues maintain a highly conserved charge for all the reaction coordinate values, indicating that these residues do not act as charge donor or acceptors in the course of the reaction.

The described charge exchange between donor and acceptor residues at the Q_o-site furthermore evidences a PCET process in the Q_o-site of the bc_1 complex which is expected to be driven by electrostatic and thermodynamic effects of the environment that surrounds the Q_o-site.

Effect of Environment on PCET at the Q_o-Site. The total energy of the system measured for different redox states of the Q_o-site allows the free energy of the PCET reaction to be established. For this purpose, the total energy of the system in the reactant state must be established, and compared to the energy of the system in the product state. In the present investigations, MD simulations were performed, considering the system as it resembles the reactant and the product states, and a reaction coordinate, ΔE, was defined as the energy difference between the reactant and the product state. This definition of the reaction coordinate is in general used for free energy calculations of charge transfer reactions,[43] as it allows the free energy to be described in terms of energy differences between reactant and product states.

Since the PCET reaction is essentially a quantum mechanical process taking place at the Q_o-site, one needs to differentiate the Q_o-site from its environment in the different redox states of the bc_1 complex. The Q_o-site model is defined here according to

DOI: 10.1021/acs.jpcb.6b07394
J. Phys. Chem. B 2016, 120, 11369−11380

its involvement in the quantum mechanical process, and it includes the atoms that have been considered in the QC calculations, as shown in Figure 2. The environment surrounding the Q_o-site, on the other hand, is composed of the remaining protein, lipids, water, and ion atoms that have been considered in the MD simulations; see Figure 6a. The total energy of the system can, therefore, be described as the sum of the energy of the Q_o-site E_{Q_o}, the energy of the environment E_{Env}, and the interaction energy between the Q_o-site and the environment E_{int}, as

$$E_{total} = E_{Q_o} + E_{Env} + E_{int} \tag{3}$$

The total energy of the system is then calculated from the classical MD simulation, using the force field approximation, for every frame of the MD trajectories. However, an additional correction to the energy has to be taken into account, as the PCET could not be described by classical mechanics but instead quantum mechanically. This means that the energy of the Q_o-site in eq 3, obtained from MD simulations, should be replaced by the QC energy of the Q_o-site, and thus the total energy of the system is

$$E_{total} = E_{total}^{(MD)} - E_{Q_o}^{(MD)} + E_{Q_o}^{(QC)} \tag{4}$$

Here, the superscript (MD) indicates that the energy was calculated from MD trajectories, while the superscript (QC) indicates that this was obtained from QC calculations.

In order to obtain the reaction coordinate for the free energy calculation, i.e., the energy differences ΔE between the reactant and product states, the calculation of the total energy in eq 4 is performed for the reactant and product states of the system for every frame in the refined 80 ns long MD trajectories (see Table 1).

For every frame of the MD trajectory in which the system is in the reactant state, one considers two redox states of the Q_o-site, while keeping the environment in the reactant state. The energy difference, thus, corresponds to the total energy difference between the two configurations of the system where the Q_o-site has been changed upon the PCET reaction, while the environment did not have enough time to respond to these changes. The energy difference thus reads as

$$\Delta E^{R} = E_{total}^{RP} - E_{total}^{RR} \tag{5}$$

where the first letter in the superscript indicates the redox state of the environment (R ≡ reactant), and the second superscript corresponds to the redox state of the Q_o-site (R ≡ reactant; P ≡ product). The energy E_{total}^{RR} is readily obtained from MD simulations corrected through QC calculations employing eq 4. To calculate the energy E_{total}^{RP}, it is required to set the atomic charges of the atoms in the Q_o-site to the values that correspond to the product state, while preserving the positions and charges of the atoms of the environment as in the reactant state simulations. In other words, E_{total}^{RP} could be obtained once the system resembles an environment of the reactant state and the Q_o-site of the product state. Analogous calculations are carried out for the product state, in which case the energy difference is

$$\Delta E^{P} = E_{total}^{PR} - E_{total}^{PP} \tag{6}$$

Once the energy differences ΔE^{R} and ΔE^{P} are obtained for the 80 ns long MD trajectories of the reactant and product states, it is possible to compare the probability distribution of the energy differences for both states of the bc_1 complex, as shown in Figure 6b. The distributions $p(\Delta E^{R})$ and $p(\Delta E^{P})$ are expected to follow the Gaussian profile

$$p(\Delta E^{i}) = \sqrt{\frac{2}{\pi\sigma_i^{2}}}\ \exp\left(-\frac{2(\Delta E^{i} - \mu_i)^2}{\sigma_i^{2}}\right) \tag{7}$$

where the superindex i corresponds to R (reactant) or P (product) states, σ_i is the width, and μ_i is the average energy difference of the distribution $p(\Delta E^{i})$. The free energy could be readily calculated once $p(\Delta E^{R})$ and $p(\Delta E^{P})$ are known:[43]

$$G^{i}(\Delta E^{i}) = -k_B T \ln p(\Delta E^{i}) \tag{8}$$

Here the superscript i stands for P (product) and R (reactant) states. Figure 6c shows the resulting free energy curves. The definition of the free energy in eq 7 implies that the energy profiles for the reactant and product states cross at $\Delta E = 0$; this is achieved by shifting the energy of one state in reference to the other. The resulting free energy profiles presented as a function of the energy difference indicate that the rate of the backward PCET process differs from the rate of the forward PCET process, which could be concluded from the asymmetry of the two energy curves in Figure 6c. Moreover, the relative position of the curve minima indicates that the PCET appears to be energetically a downhill process. This result should be differentiated from the energy profile described by the pure QC calculations in Figure 3, as the latter only describes a single conformation of the system, while the free energy calculations take into account the environment of the Q_o-site and provide a statistical averaging over a considerable number of possible configurations, that the system could populate.

The free energies obtained in this study are intended to further characterize the primary PCET at the Q_o-site of the bc_1 complex, and can be used to obtain the rate constants of the underlying charge transfer processes. However, further calculations of the PCET rate constants require additional information such as establishing the adiabaticity regime in which the reactions occur, the coupling of the quantum states that describe the system in the reactant and product states, and possibly extending MD simulations as well as performing multiple calculations for the different configurations of the Q_o-site.

Key Role of E295 and Y147. In a previous study,[10] based on MD simulations and QC computations of the Q_o-site of the bc_1 complex, it was demonstrated that the residues E295 and Y147 feature rearrangements to form a hydrogen bonding network with QH_2. In the present MD simulations, the Y147 residue occasionally turns away from the QH_2 headgroup, letting a water molecule occupy its place instead. In order to study the specific role of E295 and Y147 in the PCET process, the Q_o-site model I was modified such that (i) both residues (E295 and Y147) were removed and (ii) the Y147 residue was replaced by a water molecule.

The TS of the PCET reaction could not be established once the Q_o-site was missing the E295 residue, indicating that in this case the charge transfer reaction is energetically unfavorable, or even impossible. On the contrary, once E295 is present but Y147 is replaced by a H_2O molecule, the TS could be found from QC calculations. The energy profile of the corresponding charge transfer reaction is shown in Figure 7, where the optimized structures for the reactant and product states are indicated in the upper panels.

DOI: 10.1021/acs.jpcb.6b07394
J. Phys. Chem. B 2016, 120, 11369−11380

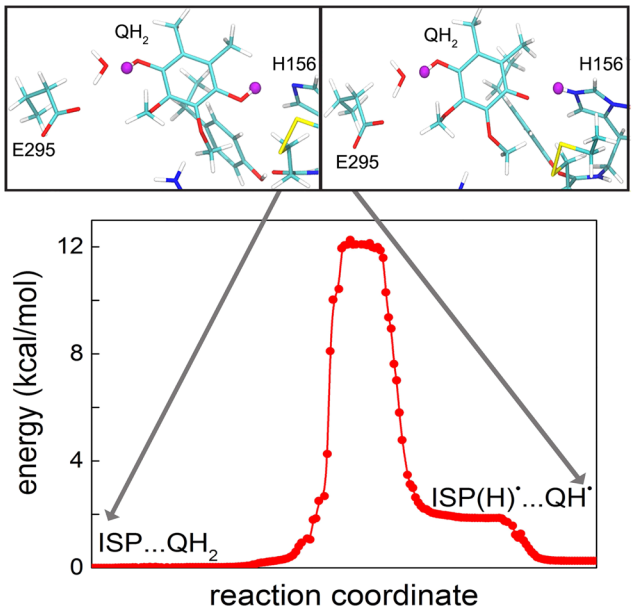

Figure 7. Minor impact of Y147 on the primary charge transfer reaction. Energy profile of the PCET reaction obtained through QC optimization of the TS by using the B3LYP/6-311G(d) method in model I and substituting Y147 by a water molecule. Labels indicate the redox states of the initial reactants and final reaction products, depicted in the upper panels. Residue E295, kept in this calculation, is still necessary for the reaction to take place, as its removal from the Q_o-site renders the proton-coupled electron transfer unlikely.

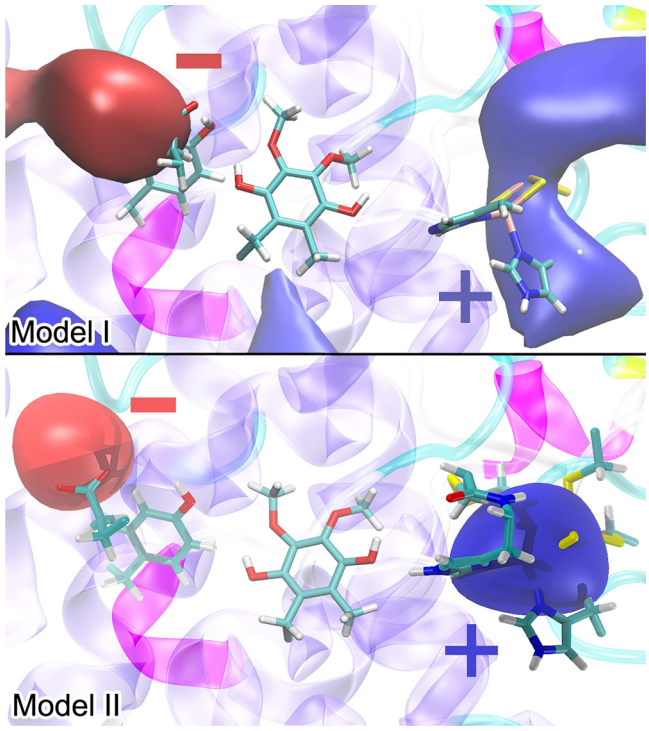

Figure 8. Electron transfer driving force. Averaged electrostatic potential at the Q_o-site of the bc_1 complex calculated from a 360 ns MD trajectory for model I and model II. The averaged negative electrostatic potentials are shown as red surfaces (equipotential value −13.1 kT/e for model I and −19.1 kT/e for model II), while blue represents surfaces of positive electrostatic potential (equipotential value +22.2 kT/e for model I and +40.5 kT/e for model II). In both models, the electrostatic potential in the reactant configuration, before any charge transfer reaction, identifies a driving force for the electron directed toward the Fe_2S_2 cluster electron acceptor.

The findings provide further support for previous investigations in which it was suggested that E295 acts as a proton acceptor, while Y147 does not play a fundamental role in the QH_2 binding or proton transfer from QH_2. However, all calculations where Y147 is present indicate a mediation of this residue in the QH_2 binding as well as in the subsequent proton transfer. The findings thus strongly suggest that Y147 acts as an intermediate bridge for the proton transfer between QH_2 and E295.

It is remarkable that the energy profile in Figure 7 is largely similar to the energy profile calculated for the complete Q_o-site model I shown in Figure 3, which indicates that the charge transfer reactions at the Q_o-site are possible even in the absence of Y147 at the Q_o-site. The E295 residue, however, is essential for the reaction to occur, as its mutation could lead to the prevention of the primary PCET reaction.

Electrostatic Potential Distribution at the Q_o-Site. Since the primary charge transfer reaction at the Q_o-site of the bc_1 complex seems to be affected by the E295 residue, one should expect that its electrostatic properties should contribute greatly to the generation of a proper electrostatic environment for rendering the primary charge transfer reactions from QH_2 to the ISP.

Earlier 360 ns long MD simulations[10] were employed here to compute the time averaged electrostatic potential of the Q_o-site for the two studied models. Figure 8 shows two well-defined positive and negative electrostatic potential regions around the QH_2 headgroup: the negative potential (red surface) is strategically centered around the side chain of E295, and the positive potential (blue surface) embraces the iron−sulfur cluster. This particular electrostatic potential distribution can produce a driving force for the valence electron of the QH_2 headgroup, indicating that it may be the key element that enables its transfer to the ISP.

As the repulsive force generated by the negative electrostatic potential, localized near the E295 residue, drives the valence electron toward the acceptor Fe_2S_2, it would seem that the PCET is initiated by the electron transfer that consequently drives a proton transfer. However, a more detailed analysis is called for at this point, in which the adiabaticity of the electron and proton transfers are accurately evaluated considering the present results.

■ CONCLUSIONS

The present study shows the coupled nature of the primary proton and electron transfer (PCET) reactions that initiate the Q-cycle at the Q_o-site of the *Rhodobacter capsulatus* bc_1 complex. This PCET process was established through the detailed analysis of reaction energetics, computed quantum mechanically for possible charge transfer reactions from the QH_2 to the Fe_2S_2 cluster of the ISP subunit in the bc_1 complex, featuring two different models of the Q_o-site, which differ in the protonation state of the key H156 residue. Particularly, for the deprotonated H156 model, which seems to support a more stable reaction, the charge delocalization at the Q_o-site indicates that an electron and a proton from the QH_2 molecule are transferred in tandem, driven by a specific electrostatic potential distribution at the Q_o-site.

DOI: 10.1021/acs.jpcb.6b07394
J. Phys. Chem. B 2016, 120, 11369−11380

The involvement of key residues, such as H156 of the ISP subunit and Y147 and E295 of the cyt. *b* subunit, in the primary PCET reaction is further elaborated, as previous MD analysis had indicated their importance.[10] The Y147 and E295 residues rearrange to form hydrogen bonds with the QH_2, and assist the second proton transfer from QH_2, which is expected to flow, toward Y147 and subsequently E295.

Free energy calculations obtained for the PCET process at the Q_o-site showed that the molecular environment of the Q_o-site plays an important role in the PCET energetics and the driving force of the reaction. The performed free energy calculations illustrate the charge transfer processes at the Q_o-site but also suggest that, in order to obtain an accurate estimate of the PCET reaction rate constants, it is necessary to reveal the adiabaticity of the proton and electron transfers. This can, for example, be achieved by exploring the Q_o-site of the bc_1 complex through hybrid computational methods such as QM/MM[44] or a polarizable embedding approach.[45]

Although the present investigation reveals the coupled nature of the primary charge transfer reactions at the Q_o-site of the bc_1 complex, the studied physical mechanism provides only a first step toward describing fundamentally important ubiquitous mechanisms of energy transport in cellular respiration and higher photosynthetic organisms, and strives for follow up investigations.

■ ASSOCIATED CONTENT

Supporting Information

The Supporting Information is available free of charge on the ACS Publications website at DOI: 10.1021/acs.jpcb.6b07394.

The supplementary topology files used in the present investigations and additional figures (PDF)

A movie of the PCET reaction (MPG)

■ AUTHOR INFORMATION

Corresponding Author

*E-mail: ilia@sdu.dk. Phone: +45 6550 2532.

Notes

The authors declare no competing financial interest.

■ ACKNOWLEDGMENTS

The research reported here has been supported by the National Institutes of Health through grant NIH 9P41GM104601 and the National Science Foundation through grant NSF PHY0822613 to K.S. The authors acknowledge supercomputer time on Stampede provided by the Texas Advanced Computing Center (TACC) at the University of Texas at Austin through Extreme Science and Engineering Discovery Environment (XSEDE) Grant XSEDE MCA93S028 and the DeIC National HPC Centre at SDU. A.M.B. is grateful to Beckman Institute for financial support. I.A.S. is grateful for financial support from the Lundbeck Foundation and the Russian Science Foundation (Grant No. 14-12-00342).

■ REFERENCES

(1) Wikstrom, M.; Krab, K.; Saraste, M. Proton−Translocating Cytochrome Complexes. *Annu. Rev. Biochem.* **1981**, *50*, 623−655.

(2) Nicholls, D. G.; Ferguson, S. *Bioenergetics*; Academic Press: Oxford, 2013.

(3) Crofts, A. R.; Berry, E. A. Structure and Function of the Cytochrome bc_1 Complex of Mitochondria and Photosynthetic Bacteria. *Curr. Opin. Struct. Biol.* **1998**, *8*, 501−509.

(4) Cramer, W. A.; Hasan, S. S.; Yamashita, E. The Q-cycle of Cytochrome bc Complexes: A Structure Perspective. *Biochim. Biophys. Acta, Bioenerg.* **2011**, *1807*, 788−802.

(5) Crofts, A. R. Proton-coupled Electron Transfer at the Q_o-site of the bc_1 Complex Controls the Rate of Ubihydroquinone Oxidation. *Biochim. Biophys. Acta, Bioenerg.* **2004**, *1655*, 77−92.

(6) Hsueh, K.-L.; Westler, W. M.; Markley, J. L. NMR Investigations of the Rieske Protein from Thermus Thermophilus Support a Coupled Proton and Electron Transfer Mechanism. *J. Am. Chem. Soc.* **2010**, *132*, 7908−7918.

(7) Chang, C. J.; Chang, M. C.; Damrauer, N. H.; Nocera, D. G. Proton-Coupled Clectron Transfer: a Unifying Mechanism for Biological Charge Transport, Amino Acid Radical Initiation and Propagation, and Bond Making/Breaking Reactions of Water and Oxygen. *Biochim. Biophys. Acta, Bioenerg.* **2004**, *1655*, 13−28. Special issue dedicated to Jerry Babcock.

(8) Sjödin, M.; Styring, S.; Åkermark, B.; Sun, L.; Hammarström, L. Proton-Coupled Electron Transfer From Tyrosine in a Tyrosine-Ruthenium- Tris-Bipyridine Complex: Comparison with Tyrosinez Oxidation in Photosystem II. *J. Am. Chem. Soc.* **2000**, *122*, 3932−3936.

(9) Berry, E. A.; Huang, L.-S.; Saechao, L. K.; Pon, N. G.; Valkova-Valchanova, M.; Daldal, F. X-ray Structure of *Rhodobacter Capsulatus* Cytochrome bc_1: Comparison with its Mitochondrial and Chloroplast Counterparts. *Photosynth. Res.* **2004**, *81*, 251−275.

(10) Barragan, A. M.; Crofts, A. R.; Schulten, K.; Solov'yov, I. A. Identification of Ubiquinol Binding Motifs at the Qo-Site of the Cytochrome bc_1 Complex. *J. Phys. Chem. B* **2015**, *119*, 433−447.

(11) Crofts, A. R.; Hong, S.; Ugulava, N.; Barquera, B.; Gennis, R.; Guergova-Kuras, M.; Berry, E. A. Pathways for Proton Release During Ubihydroquinone Oxidation by the bc_1 Complex. *Proc. Natl. Acad. Sci. U. S. A.* **1999**, *96*, 10021−10026.

(12) Crofts, A. R.; Hong, S.; Wilson, C.; Burton, R.; Victoria, D.; Harrison, C.; Schulten, K. The Mechanism of Ubihydroquinone Oxidation at the Q_o-site of the Cytochrome bc_1 Complex. *Biochim. Biophys. Acta, Bioenerg.* **2013**, *1827*, 1362−1377.

(13) Crofts, A. R.; Barquera, B.; Gennis, R. B.; Kuras, R.; Guergova-Kuras, M.; Berry, E. A. Mechanism of Ubiquinol Oxidation by the bc_1 Complex: Different Domains of the Quinol Binding Pocket and Their Role in the Mechanism and Binding of Inhibitors. *Biochemistry* **1999**, *38*, 15807−15826.

(14) Postila, P. A.; Kaszuba, K.; Sarewicz, M.; Osyczka, A.; Vattulainen, I.; Róg, T. Key Role of Water in Proton Transfer at the Q_o-site of the Cytochrome bc_1 Complex Predicted by Atomistic Molecular Dynamics Simulations. *Biochim. Biophys. Acta, Bioenerg.* **2013**, *1827*, 761−768.

(15) Phillips, J. C.; Braun, R.; Wang, W.; Gumbart, J.; Tajkhorshid, E.; Villa, E.; Chipot, C.; Skeel, R. D.; Kalé, L.; Schulten, K. Scalable Molecular Dynamics with NAMD. *J. Comput. Chem.* **2005**, *26*, 1781−1802.

(16) Mackerell, A. D.; Feig, M.; Brooks, C. L. Extending the Treatment of Backbone Energetics in Protein Force Fields: Limitations of Gas-phase Quantum Mechanics in Reproducing Protein Conformational Distributions in Molecular Dynamics Simulations. *J. Comput. Chem.* **2004**, *25*, 1400−1415.

(17) Frisch, M. J.; Trucks, G. W.; Schlegel, H. B.; Scuseria, G. E.; Robb, M. A.; Cheeseman, J. R.; Scalmani, G.; Barone, V.; Mennucci, B.; Petersson, G. A.; et al. *Gaussian 09*, revision A. 1; Gaussian, Inc.: Wallingford, CT, 2009.

(18) Becke, A. D. Density-Functional Thermochemistry. III. The Role of Exact Exchange. *J. Chem. Phys.* **1993**, *98*, 5648−5652.

(19) Shoji, M.; Koizumi, K.; Kitagawa, Y.; Yamanaka, S.; Okumura, M.; Yamaguchi, K. Theory of Chemical Bonds in Metalloenzymes IV: Hybrid-DFT Study of Rieske-type [2Fe-2S] Clusters. *Int. J. Quantum Chem.* **2007**, *107*, 609−627.

(20) Bassan, A.; Blomberg, M. R.; Borowski, T.; Siegbahn, P. E. Oxygen Activation by Rieske Non-heme Iron Oxygenases, a Theoretical Insight. *J. Phys. Chem. B* **2004**, *108*, 13031−13041.

DOI: 10.1021/acs.jpcb.6b07394
J. Phys. Chem. B 2016, 120, 11369−11380

(21) Salomon, O.; Reiher, M.; Hess, B. A. Assertion and Validation of the Performance of the B3LYP Functional for the First Transition Metal Row and the G2 Test Set. *J. Chem. Phys.* **2002**, *117*, 4729−4737.
(22) Niu, S.; Nichols, J. A.; Ichiye, T. Optimization of Spin-unrestricted Density Functional Theory for Redox Properties of Rubredoxin Redox Site Analogues. *J. Chem. Theory Comput.* **2009**, *5*, 1361−1368.
(23) Sigfridsson, E.; Olsson, M. H.; Ryde, U. A Comparison of the Inner-sphere Reorganization Energies of Cytochromes, Iron-sulfur Clusters, and Blue Copper Proteins. *J. Phys. Chem. B* **2001**, *105*, 5546−5552.
(24) Wilkens, S. J.; Xia, B.; Weinhold, F.; Markley, J. L.; Westler, W. M. NMR Investigations of Clostridium Pasteurianum Rubredoxin. Origin of hyperfine 1H, 2H, 13C, and 15N NMR Chemical Shifts in Iron-sulfur Proteins as Determined by Comparison of Experimental Data with Hybrid Density Functional Calculations. *J. Am. Chem. Soc.* **1998**, *120*, 4806−4814.
(25) Sigfridsson, E.; Olsson, M. H.; Ryde, U. Inner-sphere Reorganization Energy of Iron-sulfur Clusters Studied with Theoretical Methods. *Inorg. Chem.* **2001**, *40*, 2509−2519.
(26) Humphrey, W.; Dalke, A.; Schulten, K. VMD − Visual Molecular Dynamics. *J. Mol. Graphics* **1996**, *14*, 33−38.
(27) Kaszuba, K.; Postila, P. A.; Cramariuc, O.; Sarewicz, M.; Osyczka, A.; Vattulainen, I.; Róg, T. Parameterization of the Prosthetic Redox Centers of the Bacterial Cytochrome bc 1 Complex for Atomistic Molecular Dynamics Simulations. *Theor. Chem. Acc.* **2013**, *132*, 1−13.
(28) Feller, S. E.; Yin, D.; Pastor, R. W.; MacKerell, A. Molecular Dynamics Simulation of Unsaturated Lipid Bilayers at Low Hydration: Parameterization and Comparison with Diffraction Studies. *Biophys. J.* **1997**, *73*, 2269−2279.
(29) Aguayo, D.; González-Nilo, F. D.; Chipot, C. Insight into the Properties of Cardiolipin Containing Bilayers from Molecular Dynamics Simulations, Using a Hybrid All-Atom/United-Atom Force Field. *J. Chem. Theory Comput.* **2012**, *8*, 1765−1773.
(30) Aksimentiev, A.; Schulten, K. Imaging *alpha*-Hemolysin with Molecular Dynamics: Ionic Conductance, Osmotic Permeability, and the Electrostatic Potential Map. *Biophys. J.* **2005**, *88*, 3745−3761.
(31) Szilagyi, R. K.; Winslow, M. A. On the Accuracy of Density Functional Theory for Iron-sulfur Clusters. *J. Comput. Chem.* **2006**, *27*, 1385−1397.
(32) Peng, C.; Bernhard Schlegel, H. Combining Synchronous Transit and Quasi-Newton Methods to Find Transition States. *Isr. J. Chem.* **1993**, *33*, 449−454.
(33) Peng, C.; Ayala, P. Y.; Schlegel, H. B.; Frisch, M. J. Using Redundant Internal Coordinates to Optimize Equilibrium Geometries and Transition States. *J. Comput. Chem.* **1996**, *17*, 49−56.
(34) Fukui, K. The Path of Chemical Reactions - the IRC Approach. *Acc. Chem. Res.* **1981**, *14*, 363−368.
(35) Hratchian, H. P.; Schlegel, H. B. In *Theory and Applications of Computational Chemistry*; Dykstra, C. E., Frenking, G., Kim, K. S., Scuseria, G. E., Eds.; Elsevier: Amsterdam, The Netherlands, 2005; Chapter 10, pp 195−249.
(36) Singh, U. C.; Kollman, P. A. An Approach to Computing Electrostatic Charges for Molecules. *J. Comput. Chem.* **1984**, *5*, 129−145.
(37) Besler, B. H.; Merz, K. M.; Kollman, P. A. Atomic charges derived from semiempirical methods. *J. Comput. Chem.* **1990**, *11*, 431−439.
(38) MacKerell, A. D.; Bashford, D.; Bellott, M.; Dunbrack, R. L.; Evanseck, J. D.; Field, M. J.; Fischer, S.; Gao, J.; Guo, H.; Ha, S.; et al. All-Atom Empirical Potential for Molecular Modeling and Dynamics Studies of Proteins. *J. Phys. Chem. B* **1998**, *102*, 3586−3616.
(39) *Mathematica*, version 10.3; Wolfram Research Inc.: Champaign, IL, 2015.
(40) Lodish, H.; Berk, A.; Zipursky, S. L.; Matsudaira, P.; Baltimore, D.; Darnell, J. *Molecular Cell Biology*, 4th ed.; WH Freeman: New York, 2000.
(41) Truhlar, D. G.; Isaacson, A. D.; Garrett, B. C. In *Theory of Chemical Reaction Dynamics*; Baer, M., Ed.; CRC Press: Boca Raton, FL, 1985; Chapter 4, pp 65−137.
(42) Hammond, B. L.; Lester, W. A., Jr; Reynolds, P. J. *Monte Carlo Methods in ab initio Quantum Chemistry*; World Scientific: Farrer Road, Singapore, 1994; Vol. *1*.
(43) Blumberger, J. Free Energies for Biological Electron Transfer from QM/MM Calculation: Method, Application and Critical Assessment. *Phys. Chem. Chem. Phys.* **2008**, *10*, 5651−5667.
(44) Warshel, A.; Levitt, M. Theoretical Studies of Enzymic Reactions: Dielectric, Electrostatic and Steric Stabilization of the Carbonium ion in the Reaction of Lysozyme. *J. Mol. Biol.* **1976**, *103*, 227−249.
(45) Olsen, J. M.; Aidas, K.; Kongsted, J. Excited States in Solution through Polarizable Embedding. *J. Chem. Theory Comput.* **2010**, *6*, 3721−3734.

DOI: 10.1021/acs.jpcb.6b07394
J. Phys. Chem. B 2016, 120, 11369−11380